International Journal of Biomedical Engineering and Technology

ISSN online: 1752-6426 - ISSN print: 1752-6418
https://www.inderscience.com/ijbet

Mammograms enhancement based on multifractal measures for microcalcifications detection

Nadia Kermouni Serradj, Sihem Lazzouni, Mahammed Messadi

DOI: 10.1504/IJBET.2023.10053531

Article History:

Received:	16 August 2020
Last revised:	23 October 2020
Accepted:	09 November 2020
Published online:	25 January 2023

Mammograms enhancement based on multifractal measures for microcalcifications detection

Nadia Kermouni Serradj*,
Sihem Lazzouni and Mahammed Messadi

Laboratory of Biomedical Engineering,
University of Tlemcen, Algeria
Email: nadia.kermouni@gmail.com
Email: sa_lazzouni@yahoo.fr
Email: mahammed.messadi@univ-tlemcen.dz
*Corresponding author

Abstract: Breast cancer is the most common cancer in women and represents as a leading cause of death in the world (https://gco.iarc.fr/today/home). Microcalcifications (MCs) are the essential signs of precancerous cells. Their small size makes them difficult to detect and locate, hence the need of developing computer-aided detection systems for early detection of breast cancer. In this paper, an approach of MCs detection is proposed. Our system includes three phases. In the first, we start by a pre-processing step to remove various noises, followed by a step of intensity enhancement based on the haze removal algorithm. The third step is based on multifractal measures to construct the α-image which enhance MCs contrast. The proposed method was tested on three databases with a set of 371 images and evaluated in terms of PSNR and sensitivity. The obtained results are very significant and better compared to other approaches proposed in the literature.

Keywords: multifractal measure; α-image; contrast enhancement; microcalcifications; mammogram filtering; mammographic images processing and breast cancer.

Reference to this paper should be made as follows: Kermouni Serradj, N., Lazzouni, S. and Messadi, M. (2023) 'Mammograms enhancement based on multifractal measures for microcalcifications detection', *Int. J. Biomedical Engineering and Technology*, Vol. 41, No. 1, pp.60–82.

Biographical notes: Nadia Kermouni Serradj is a PhD student in Biomedical Engineering at the University of Tlemcen, Algeria. She obtained her Masters in Medical Imaging in 2017 from the University of Tlemcen. Her research area focuses on medical image processing and applications.

Sihem Lazzouni is an Assistant Professor at the University of Tlemcen, Algeria. She received her Engineering degree in Electrical Engineering from University of Tlemcen in 1997. In 2006, she obtained her PhD in Electrical Engineering from the University of Tlemcen, Algeria. Her research interests are in computer vision and fractal analysis.

Mahammed Messadi is an Assistant Professor at the University of Tlemcen, Algeria. He received his Engineering in Electrical from the University of Tlemcen in 2003. In 2010, he obtained his PhD in Biomedical Engineering from the University of Tlemcen, Algeria. His research interests are in computer vision, computational intelligence (CI), image processing, neural networks and clustering methods.

1 Introduction

Breast cancer is a real public health stake. It is the most common female cancer and the leading cause of women death worldwide. In 2018, according to the International Agency for Research on Cancer (IARC) of the World Health Organization (WHO), more than 2,000,000 new cases of breast cancer in the world are registered, most of them at an advanced stage and in young age and more than 600,000 deaths are recorded by this disease (https://gco.iarc.fr/today/home). Screening for the disease and early diagnosis remain the main means to combating this scourge and reducing the rate of death.

Mammography is the main imaging modality for breast exploration that has proven its effectiveness in the diagnosis of breast cancer. However, this exam has limitations related to interpretation difficulties particularly when it concerns small lesions like microcalcifications (MCs). These difficulties are due to image quality as bad contrast, noise and artefacts, the size of the tumour, the complex anatomy of the breast, the surrounding structure, density variations, or to factors related to radiologist, such as fatigue, inattention or experience level.

MCs are the main sign of precancerous cells. They appear on mammograms as small granular bright spots of calcium deposits. They are diagnosed by analysing their morphology, distribution and sometimes change over time, described in the BI-RADS Atlas edited by the American College of Radiology (ACR). They may appear alone, scattered or in clusters typically in sizes ranging from 0.05 to 1 mm. The distribution of these calcifications can be clustered, linear, segmental or diffused (scattered). Linear as well as segmental distribution indicates malignancy while those appearing like smooth and rod-like structures are generally benign. Radiologists give special attention to scattered MCs with dimensions of 0.2 to 0.3 mm as well as those in clusters (presence of more than three MCs in an approximate area of 1 cm^2) (Bhateja et al., 2020).

Many researchers worked on the development of automatic computer-aided systems to assist radiologist in the detection and diagnosis of breast lesions and cancer in mammography using different approaches ranging from conventional image analysis methodologies to machine learning techniques (Abdallah et al., 2018; Eltrass and Salama, 2019; Mutlu et al., 2020; Bagchi et al., 2020; Al-Antari et al., 2020; Hamed et al., 2020). These systems allow increasing the cancer detection rate at an early stage and reducing false positive and false negative interpretations.

The detection of MCs is a major challenge that has been the subject of several studies. Many approaches are proposed in the literature for the segmentation, detection and characterisation of MCs. Ciecholewski (2017) and Hadjidj et al. (2019) used morphological operations and watershed method for the detection and segmentation of MCs. Quintanilla-Domínguez et al. (2018) used morphological top hat transform for contrast improvement of ROI, k-means and self-organising map (SOM) clustering algorithms for ROI segmentation and neural network for classification. Singh and Kaur (2018) proposed an approach to discriminate between malignant and benign MCs clusters where they used morphological operations for ROI enhancement, then, cluster shape and texture features are extracted for SVM classification. In Basile et al. (2019), histogram modification and spatial filtering for mammograms enhancement are used, then, Hough transform and relaxed threshold are applied for the segmentation of clusters, and clusters identification is done using Ward's hierarchical agglomerative clustering algorithm. Rubio et al. (2019) introduces a novel methodology based on quantum signal processing (QSP) and cellular automata (CA) to detect MCs in mammograms in binary and

greyscale images. Other approaches are based on multi-resolution analysis, used with unsharp masking and histogram modification for enhancement step (Alasadi and Al-Saedi, 2017), morphological analysis for cluster segmentation (Alam et al., 2018), or combined with other method as canny algorithm and Otsu thresholding (Azam et al., 2020). Most of recent works are based on deep neural network (Wang and Yang, 2018; Valvano et al., 2019; Savelli et al., 2020). Our proposed approach is based on the fractal geometry.

Fractal geometry was introduced by the mathematician Benoît Mandelbrot where he coined the term 'fractal' to describe complex structures found in nature whose Euclid geometry did not allow their description. He defined a fractal as a geometric object composed of smaller parts, where each part is a smaller copy of the whole. This property is called 'self-similarity' or 'scale invariance', it is described by the fractal dimension (FD) (Mandelbrot, 1975). Some structures are more complex where they cannot be characterised by a single FD, hence, the birth of multifractal analysis which is a generalisation of fractal analysis allowing the characterisation of irregular natural structures as a spectrum of local FDs called multifractal spectrum (Atupelage et al., 2013).

Fractal and multifractal analysis have been applied in analysing a variety of medical images using different methods (box counting, wavelet transform modulus maxima – WTMM, detrended fluctuation analysis – DFA) to estimate FD and multifractal spectrum, and have played an important role in health and medical research such as differentiating pathological tissues from healthy ones (Ţălu, 2015; Ward and Bai, 2013; Tălu et al., 2015; Ţălu et al., 2017; LolaCosta and Nogueira, 2015; Rajkovic et al., 2017; Khider, 2011; Baravalle et al., 2017; Vasiljevic et al., 2015) and diagnosis of some diseases (Rajković et al., 2016; Rajkovic et al., 2017). It has also been successfully used in detection and segmentation of variety of medical images (Jayasuriya et al., 2013; Yu et al., 2015; Bhat et al., 2017; Ding et al., 2016). In mammography, fractal analysis using box counting method to estimate FD has been used for classification of breast ultrasound images (Chen et al., 2005), classification of breast masses (Rangayyan and Nguyen, 2005), characterisation and classification of breast cancer (Li et al., 2007; Mohammed et al., 2018), characterisation of MCs (Verma et al., 2018) and detection of architectural distortion (Zyout and Togneri, 2018). However, multifractal analysis has been applied to digital mammograms for the segmentation of MCs using box counting method (Stojić et al., 2006; Sahli et al., 2015) and for differentiating between the fatty tissue and the dense tissue and discriminating between malign and benign cases using WTMM method (Kestener et al., 2001; Kestener, 2003; Gerasimova-Chechkina et al., 2016; Marin et al., 2017). Recently, Slim et al. (2019) proposed an approach for segmentation of MCs based on the construction of α_image from multifractal spectrum of the original image and the construction of $f(\alpha)$_image from the global regularity measure of α_image using the box counting method to calculate FD and gliding box method to measure lacunarity. This approach was applied only to the region of interest containing MCs and no evaluation was made to assess the results. Another fractal approach was proposed in Datta and Sathish (2019) to locate the MCs in mammogram where authors used the FD estimated by the box counting method and the Hurst exponent with Sobel and morphological operators to segmentation of the mammogram and localisation of MCs. Sanchez-Montero et al. (2019) propose a method for filtering mammograms using convolution with directional fractal masks to enhance MCs in full mammograms.

Most of approaches proposed in the literature whether for detection or segmentation of MCs work directly on the region of interest, extracted automatically or manually according to the expert. Also, the recently proposed computer-aided detection (CAD) systems based on machine learning techniques require a large labelled database for the training step and robust hardware. On the other hand, according to the literature, fractal and multifractal methods do not require pre-processing steps since they study the variation of the function from one point to another. In this paper, we develop a mammogram filtering approach combined with a multifractal method for the visualisation and detection of MCs. For filtering step, we used haze removal technique to reduce the breast density which constitutes a real obstacle for radiologists when locating MCs especially in cases where the density is higher. Then, the box counting method for estimation of local FDs is used to construct the α-image of the full mammogram that allows to highlight the MCs from surrounding tissue. The obtained results show that the contrast of MCs has been well enhanced so that they can be easily detected and located by the radiologist.

The paper is organised in four sections. The databases and proposed approach for MCs detection are discussed in Section 2. Section 3 presents the discussion of the obtained results. Finally, conclusions are reported in Section 4.

2 Experimental method

In this paper, we develop a filtering approach for the MCs visualisation and detection. Our approach based on multifractal analysis aims to provide a fast and accurate detection of the MCs in mammographic images.

2.1 Database description

There are several public mammography databases. The most used in literature are: Mammographic Image Analysis Society (MIAS) database, Digital Database for Screening Mammography (DDSM), INbreast database and Breast Cancer Digital Repository (BCDR) (Lopez et al., 2012). Figure 1 shows an example of the three bases used in this paper.

2.1.1 Minis-MIAS database

The MIAS Digital Mammogram Database is the oldest available database and the widely used in literature. It contains 322 digitised MLO images sized in 1,024 × 1,024 pixels in grey levels. There are 209 normal cases and 113 pathological cases with all types of findings (mass, calcification, architectural distortion, asymmetry), specifying benign and malign lesions and breast density information but not classified according to the BI-RADS standards. The list is arranged in pairs of films, where each pair represents the left and right mammograms of a single patient (http://peipa.essex.ac.uk/info/mias.html). It contains 23 cases of calcifications.

Figure 1 Examples of mammograms of different databases used (a) mini-MIAS, (b) DDSM and (c) INBreast

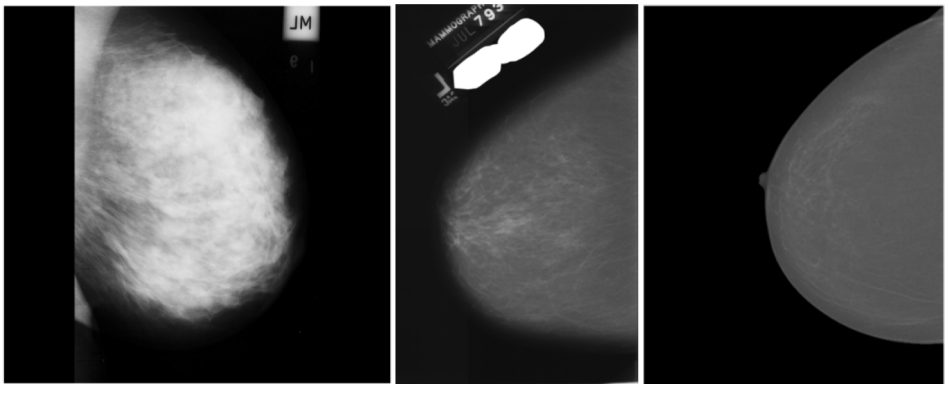

(a) (b) (c)

Table 1 Quantitative description of databases

Database	*Normal mammograms*	*Pathological mammograms*	*MCs mammograms*
MIAS	209	113	23
DDSM	2,780	7,700	1,856
INbreast	67	343	308

2.1.2 DDSM database

DDSM is the largest mammogram database with 2,620 cases including two images from each breast: left and right, each breast is taken in two catches: MLO and CC, for a total of 10,480 images including 2,780 normal mammograms and 7,700 pathological mammograms with all types of findings specifying benign and malign lesions, the breast density and assessment according to BIRADS standards. In addition, the date of study, patient age and the digitiser are also mentioned (Heath et al., 1998). The database contains 1,856 mammograms with MCs.

2.1.3 INbreast database

The database was acquired at the Breast Center of Porto. It contains 410 images. Each image matrix is 3,328 × 4,084 or 2,560 × 3,328 pixels saved in DICOM format. The database includes normal mammograms and mammograms with all types of findings. Each finding has a label that identifies the type of lesion. It contains 308 images of calcifications (Moreira et al., 2012).

However, each database has strengths and limits in terms of image resolution, case description and most importantly the segmentation of the expert. Interesting by the detection of MCs, the INbreast database provides the best segmentation with the exact position of the MCs. Table 2 summarises the strengths and limits of each database.

Table 2 Advantages and limits of each database

Database	*Strengths*	*Limits*
MIAS	Available search system.	Low resolution
		Absence of CC view
		Absence of BI-RADS classification
		Insufficient annotations (absent in case of widely distributed calcifications)
DDSM	Large number of cases.	Non-standard format
	Detailed description of the lesion.	Insufficient annotations
		Unavailable search system
INbreast	High resolution	Findings notes in Portuguese
	Exact positions of lesions.	
	Available search system.	

2.2 Proposed method

In this paper, we propose an approach of filtering full mammograms for MCs detection. Figure 2 details the global diagram of the proposed approach.

Figure 2 Global diagram of the proposed approach

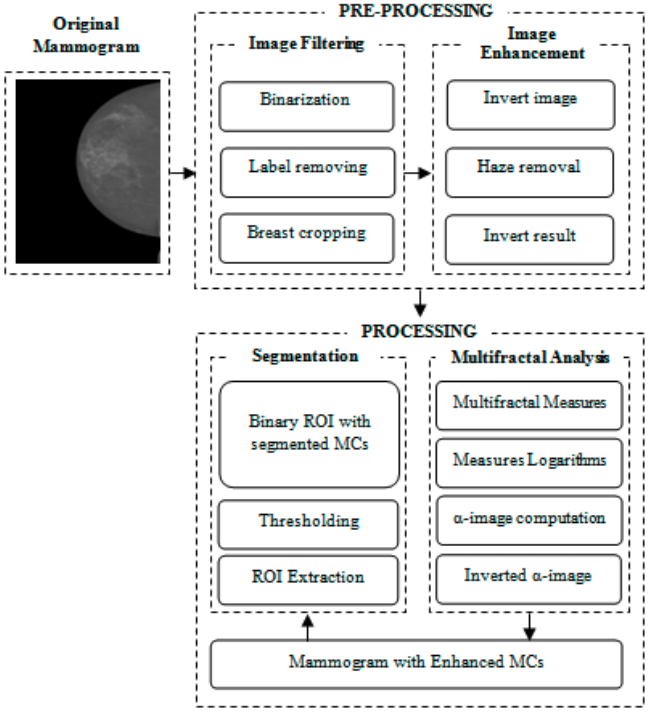

Figure 3 Image binarisation step, (a) original mammogram (b) corresponded histogram (c) thresholding image (see online version for colours)

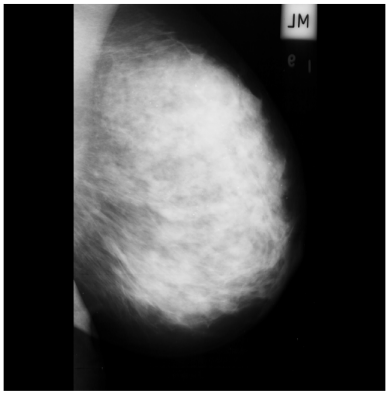

(a)

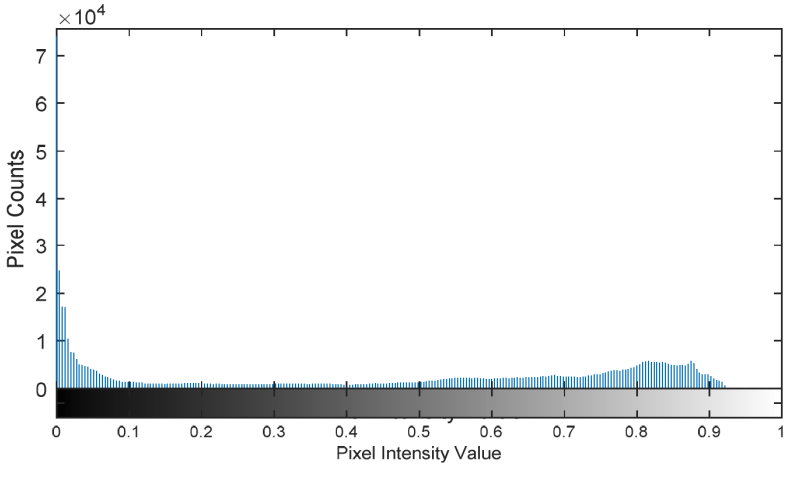

(b)

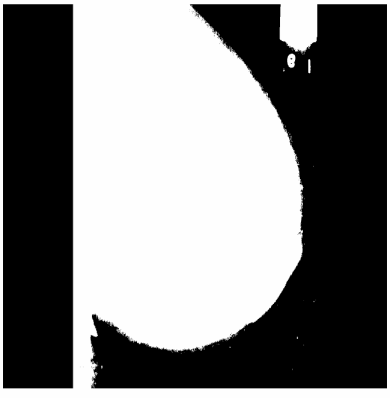

(c)

Figure 4 Breast zone selction step, (a) labelled binary image (b) breast binary mask (c) result of convolution original image and breast mask (d) cropped image (see online version for colours)

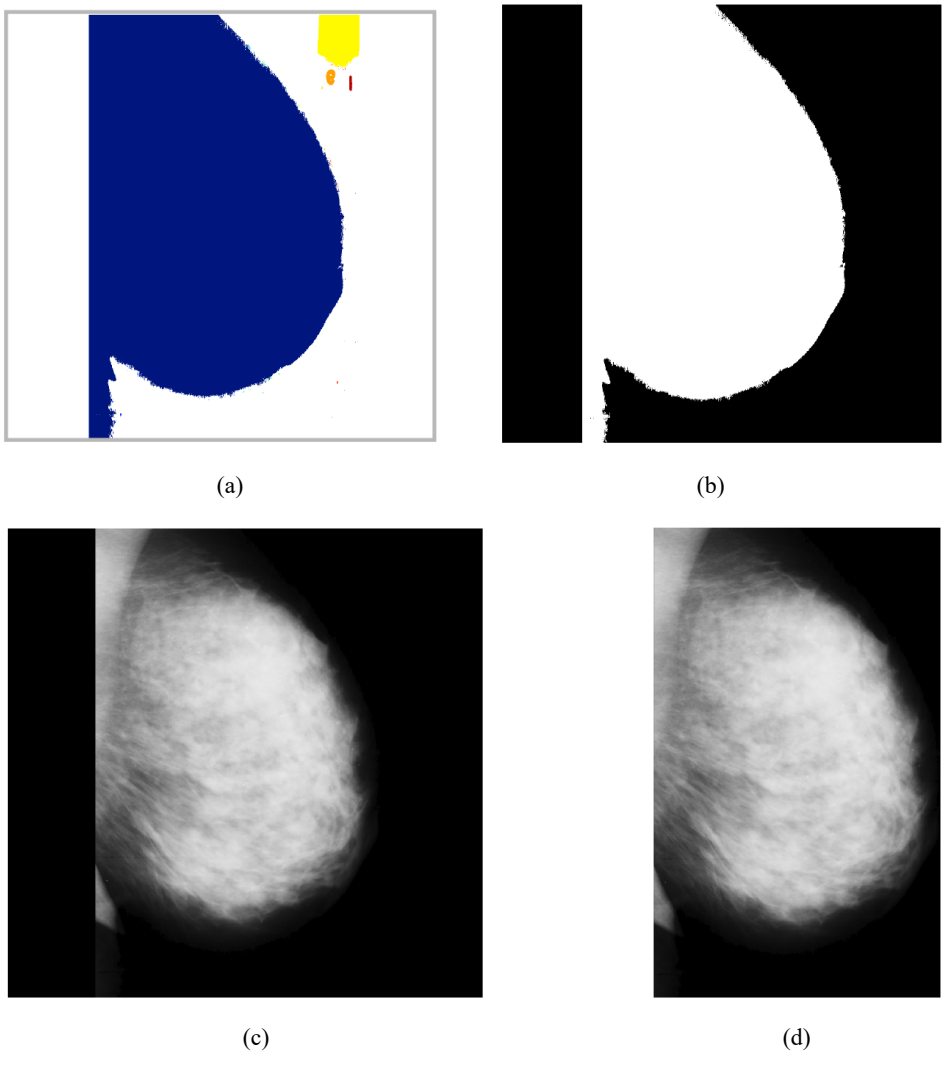

(a) (b)

(c) (d)

2.2.1 Mammogram filtering

- Image binarisation

  From the histogram of original images, the threshold value is set so as to separate the black background corresponding to the values between [0–0.02] from the other structures of the mammography (> 0.02) (Figure 3).

- Breast zone selection

  The image obtained by thresholding is composed of several connected components corresponding to the breast area, labels and artefacts. In order to keep only the breast

which represents the large connected component, the image obtained by thresholding is labelled [Figure 4(a)] and the area of each label (object) is calculated. The breast mask corresponds to the large area [Figure 4(b)]. Finally, the breast zone image is obtained by convolving obtained mask and the original image [Figure 4(c)].

- Image cropping

  In order to reduce computation time of the next steps, the filtered mammogram is cropped by removing empty rows and columns which represent the surplus of background of the mammogram (represented in black) and keep only the breast without affecting it [(Figure 4(d)].

  The idea is to initialise a null matrix (T) of the same size as the filtered image (I), find the empty rows of the filtered image $I(i, :)$ which are equal to $T(i, :)$ and store them in a vector, the same procedure is done for the columns. Finally, the row and column vectors are removed from the filtered image.

2.2.2 Low-light image enhancement

To reduce breast density and highlight MCs in relation to density, we use a low-light image enhancement algorithm based on haze removal technique (https://fr.mathworks.com/help/images/low-light-image-enhancement.html) because breast density can be considered as haze in mammography. The enhancing results are shown in Figure 5. These comprise three steps:

- Invert the filtered mammogram (J):

  $$I = 1 - J$$

- Apply the haze removal algorithm to the inverted image (He et al., 2010): The model to describe a hazy image I is:

  $$I(x) = J(x)T(x) + L\left(1 - T(x)\right)$$

  I is the observed intensity, J is the scene radiance, L is atmospheric light, and T is a transmission map describing the portion of light that reaches the camera.

  In this paper, we used the MATLAB function 'imreducehaze'. It follows these steps:

  1 estimate the atmospheric light L
  2 estimate the transmission T
  3 refine the estimated transmission map
  4 recover scene radiance
  5 restore the image
  6 perform optional contrast enhancement to obtain the enhanced image with removed haze.

- Invert the enhanced image:

  $$K = 1 - enhanced\_image$$

Figure 5 Mammogram enhancing, (a) filtered mammogram (b) inverted filtered mammogram (c) breast density removing using haze removal technique (d) enhanced mammogram

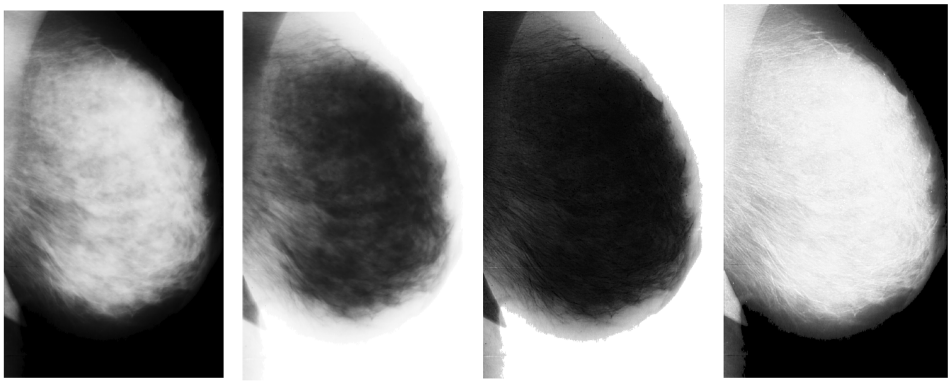

(a) (b) (c) (d)

2.2.3 Multifractal measures: α-image

Multifractal analysis consists to describe the properties of local singularity, called Hölder's exponent or α-value, using a measure estimated from the intensity of the neighbouring pixels. This coefficient reflects the local behaviour of a function $\mu_p(w)$ [equation (1)] around the pixel, where w is the size of the box centred at the pixel p (Figure 6). The variation of the intensity measure with respect to w can be estimated as follows (Chianghau, 2012):

$$\mu_p(w) = Cw^{\alpha_p} \tag{1}$$

$$\alpha_p(m,n) = \frac{\ln\left(\mu_p(m,n)\right)}{\ln(w)} \tag{2}$$

where C is an arbitrary constant.

Figure 6 Different size of windows of centred pixel in red, (a) $w = 1$ (b) $w = 3$ (c) $w = 5$ (see online version for colours)

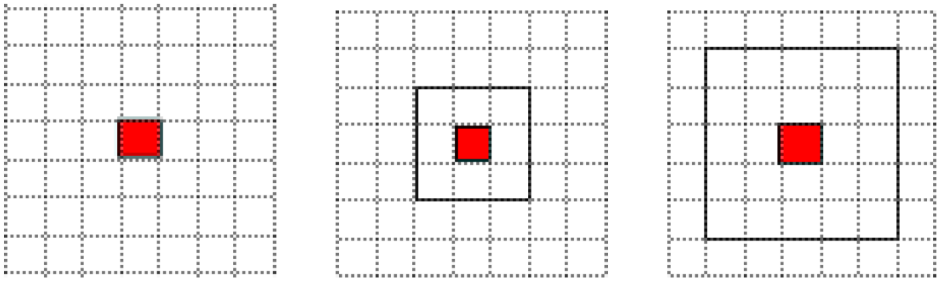

(a) (b) (c)

Notes: $w = 2i + 1$, $i = 0, 1, 2, \ldots d$, d is the total number of windows.

Different measures $\mu_P(m, n)$, may be used for estimating α-value: maximum measure, inverse-minimum measure, summation measure, iso-measure, absolute difference, central absolute difference, maximum summation difference and modified iso-measure (Stojić et al., 2006).

In this paper, we use the inverse minimum measure. Let $g(k, l)$ represent the intensity value at pixel (m, n), and Ω the set of all pixels within the measured neighbourhood of a square window of size w, the inverse minimum measure (Chianghau, 2012):

$$Inv - \min : \mu_w(m, n) = 1 - \min g(k, l), (k, l) \in \Omega \tag{3}$$

For estimating Hölder exponents α_p, natural logarithms of measure value $\ln(\mu_p(m, n))$ and of the window size $\ln(w)$ [equation (2)] are calculated and plotted corresponding points in bi-logarithmic diagram $\ln(\mu_p(m, n))$ vs. $\ln(w)$. Then, the limiting value of $\alpha(m, n)$ is estimated as a slope of linear regression line (Stojić et al., 2006).

The computation of local singularities of the original image produces the α-image: it is a two-dimensional matrix where each α-value in α-image corresponds to pixel value on the original image. The α-image is inverted to obtain the enhanced mammogram which highlights the MCs for their detection.

Figure 7 Final result of the proposed approach, (a) original mammogram (b) α-image (c) inverted α-image

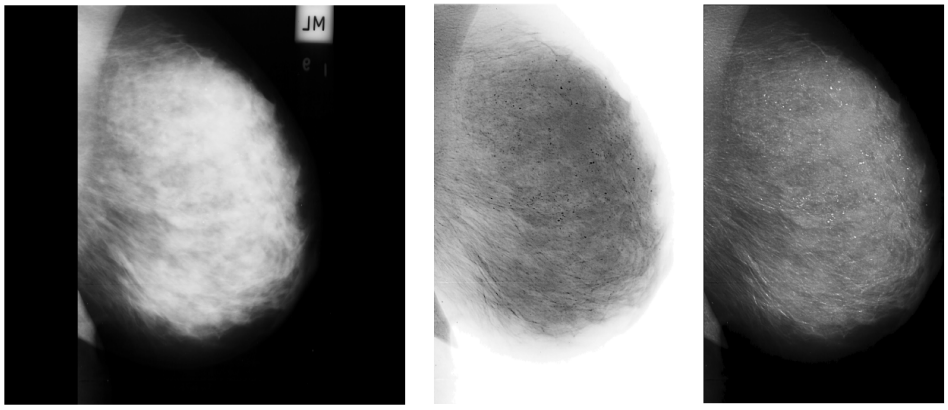

(a) (b) (c)

Illustrative example

Step 1 Load the processed image.

Step 2 Conversion to double precision and normalisation.

Step 3 Mutlifractal measure of each windows.

For each window, the centred pixel is replaced by the multifractal measure.

Step 4 Natural logarithm of each measure matrix.

Step 5 α-image obtained by linear regression.

Figure 8 Illustrative example of the first and the second step

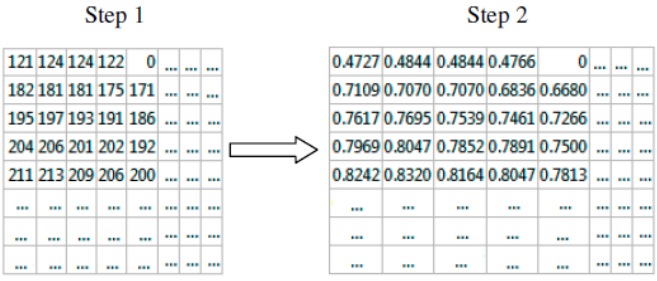

Figure 9 Computation of the multifractal measures using 3 sliding windows of different size (step 3) (see online version for colours)

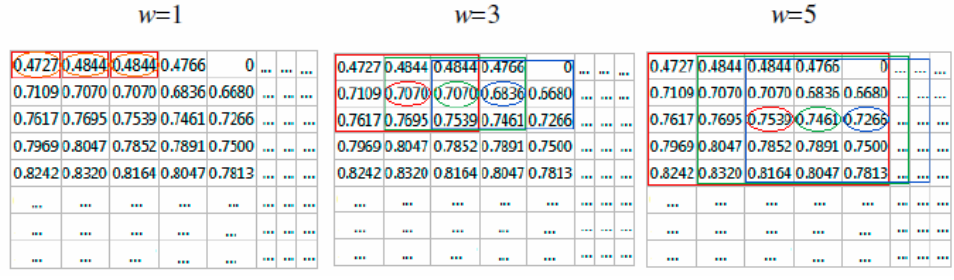

Figure 10 Natural logarithm of each measure matrix (step 4)

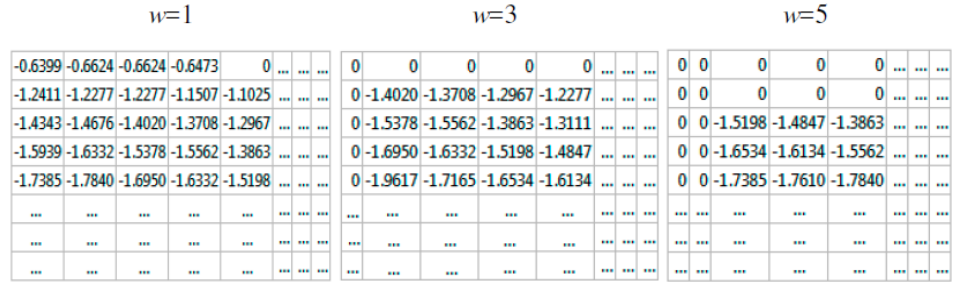

Figure 11 Obtained α-image by the linear regression (step 5) and the result of it inversion and conversion (step 6)

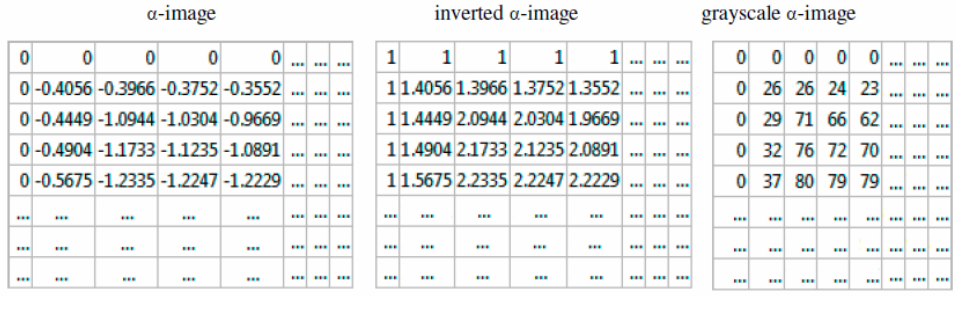

Step 6 Invert the α-image and convert it to an integer greyscale image with pixel intensities in range [0 255] to obtain the final result of enhanced mammogram.

To avoid log (0), measures equal to 0 are kept at 0.

Figure 12 Case '20587320' of INbreast database, (a) original mammogram (b) original ROI (c) enhanced mammogram (d) enhanced ROI with highlighted MCs (see online version for colours)

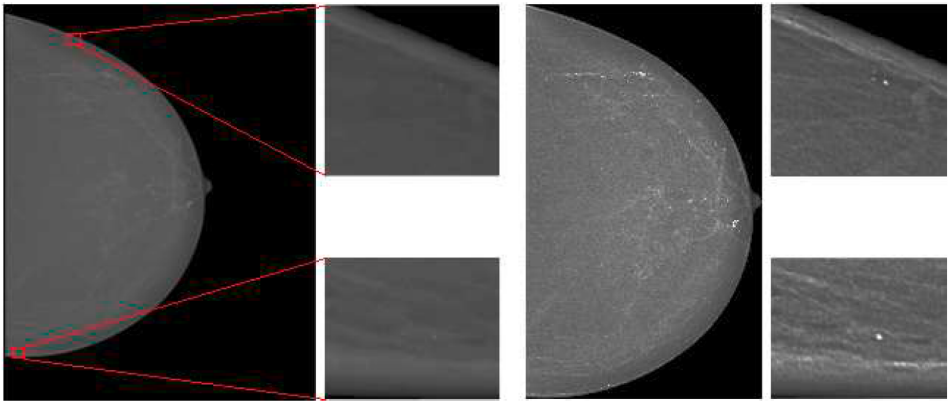

(a) (b) (c) (d)

3 Results and discussion

The proposed method was tested using the three databases presented previously. The INbreast database was used to study the ability and quality of MCs enhancement in relation to breast density. The other two databases were used only for the estimation of detection sensitivity.

For this, all mammograms of INbreast database containing MCs (308 mammograms) were sorted and classified according to the BI-RADS classification of the breast density into four classes: class A < 25%, class B between 25% and 50%, class C between 50% and 75% and class D > 75% breast density. Figure 13 describes the number of mammograms of each class BI-RADS.

Figure 13 Reorganisation and classification of mammograms images containing MCs according to BI-RADS classification (see online version for colours)

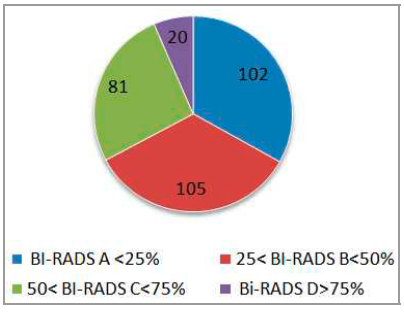

The algorithm was implemented on MATLAB R2019b using a laptop which has a processor Intel(R) Core(TM) i5-3230M CPU and NVIDIA Optimus graphics card.

In order to validate our results, the proposed method was evaluated in the terms of image quality and sensitivity.

3.1 Image quality analysis:

There are several measures to quantify the quality of an image. In order to compare our results with those of the literature, we calculated the peak signal to noise ratio (PSNR) which measures the quality of the processed image compared to the original image:

$$PSNR = 10\log_{10}\left(\frac{MAX_I}{MSE}\right) \tag{4}$$

where MAX_I is the maximum possible pixel value of the image, MSE is the mean square error between processed and original image.

The PSNR was calculated for the proposed approach and compared with the PSNR calculated for contrast-limited adaptive histogram equalisation (CLAHE) method.

Figure 14 Case '20587544' of INbreast database, (a) original image (b) filtered image (c) result of CLAHE method (d) result of the proposed method

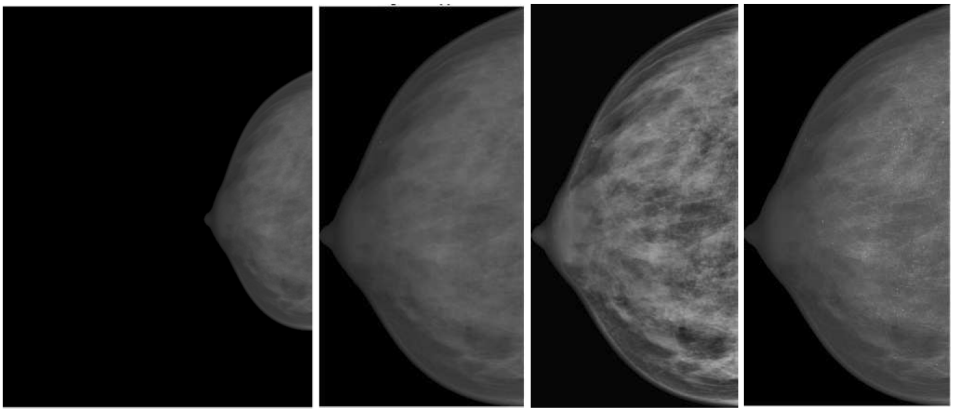

(a) (b) (c) (d)

Figure 15 illustrates the PSNR graphs obtained for each class. We note that for the four classes, the PSNR of the proposed method is higher than that of the CLAHE method.

Table 3 PSNR mean values for each BI-RADS class

BI-RADS classes	*Images number*	*Mean PSNR (CLAHE, original)*	*Mean PSNR (α-image, original)*
BI-RADS A	102	25.1439132	26.1159662
BI-RADS B	105	24.1541365	25.4004571
BI-RADS C	81	23.3214791	25.4079568
BI-RADS D	20	22.49564575	26.7863911

Figure 15 Illustration of PSNR graphs of each BI-RADS class (see online version for colours)

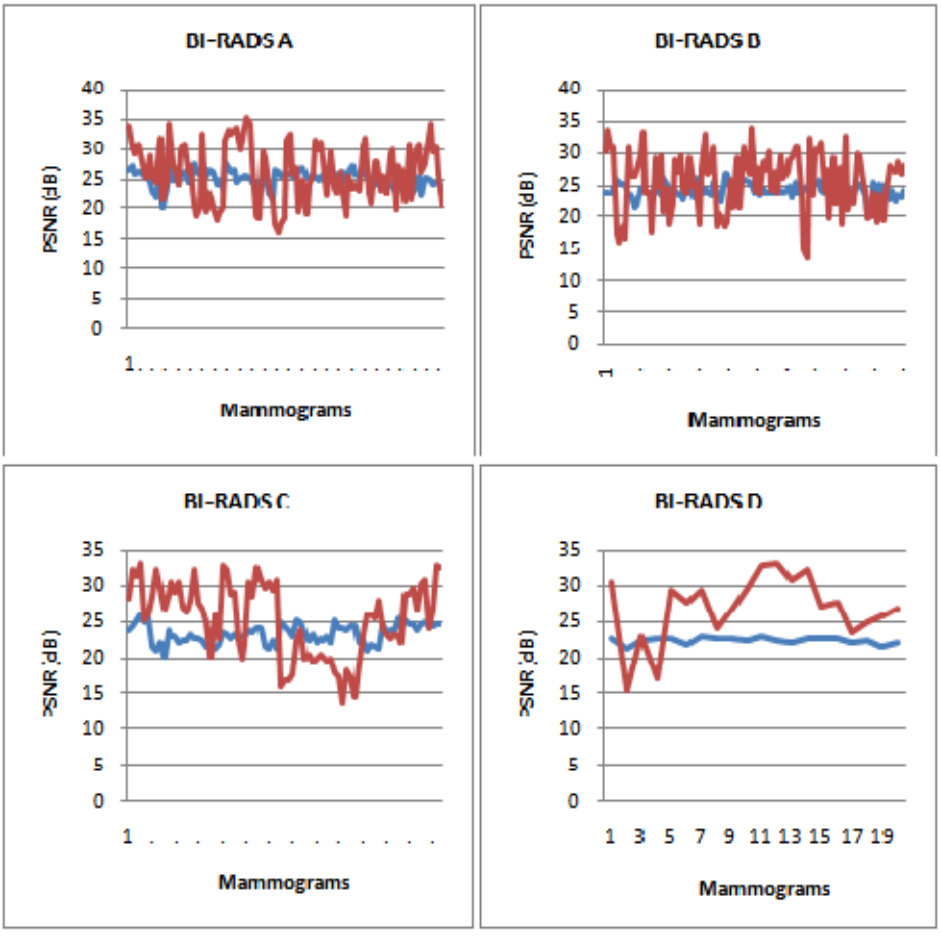

Notes: The blue graphs represent the PSNR (CLAHE, original) and the red graphs represent the PSNR (α-image, original).

A higher PSNR means that the image contains more signal than noise in the image. In our hypothesis, breast density is considered to be noise, especially in cases of classes C and D where the density is high (> 50%) and can mask MCs which are the essential information that we are trying to detect. As already explained in the previous section, we proposed a pre-processing step for reducing breast density by taking inspiration from the technique of haze removal in atmospheric images.

Therefore, the high PSNR values obtained by the proposed method justify that the breast density has been attenuated and the MCs have been revealed by the α-image. This is particularly remarkable in the PSNR mean values of C and D classes where the difference between the values of the proposed method and the CLAHE method is significant and proves that the contrast has been increased between MCs and surrounding tissues which allows a better distinction of MCs.

3.2 ROI analysis

To evaluate the quality of MCs enhancement region over the surrounding tissue, we calculate the PSNR of ROI using the follower formula (Sanchez-Montero et al., 2019):

$$PSNR = \frac{p-b}{\sigma} \tag{5}$$

where p is the maximum grey-level value of the MC area, b is the mean grey-level value of the background and σ is the standard deviation in the background region.

Figure 16 ROI analysis, (a) original ROI (b) CLAHE ROI (c) ROI of the proposed method

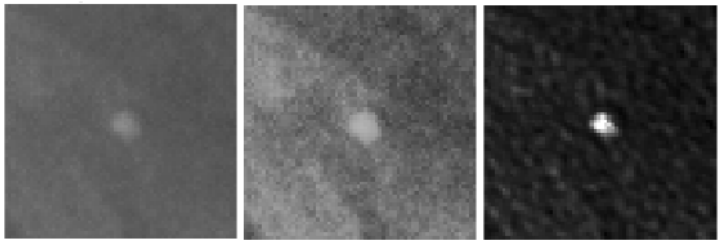

(a) (b) (c)

Figure 17 Illustration of PSNR graphs of different ROIs (see online version for colours)

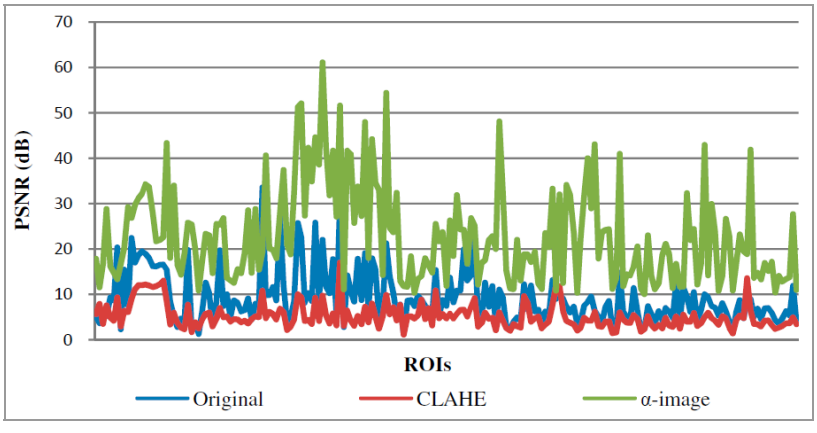

PSNR values of ROIs were calculated for the original ROI, ROI obtained with CLAHE and ROI of our proposed method (Figure 16). The size of each ROI is 32 × 32. Figure 17 illustrates the PSNR graphs of the original ROI, CLAHE ROI and ROI of the proposed method.

In Table 4, we presented the mean PSNR values of each class, these values are compared with others methods presented in literature (Table 5). According to this comparison, our approach gives the better results for MCs detection in mammography images (Table 5).

Table 4 Mean PSNR values of ROIs for each BI-RADS class

BI-RADS class	*Number of ROIs*	*Original ROI*	*CLAHE ROI*	*Prop. method ROI*
A	824	7.82	8.08	33.99
B	379	7.65	4.34	13.62
C	285	6.03	3.80	16.88
D	223	4.35	3.26	21.15

Table 5 Comparative mean PSNR values

Research	*Database*	*Number of mammograms*	*Mean PSNR*
Sanchez-Montero et al. (2019)	Private + BCDR	40	18.74
Proposed method	INbreast	**308 (1,711 ROIs)**	**24.97**

In this part, the calculation of the PSNR is based on the difference between the max value of MC and the mean value of the background. If this difference is great, so is the PSNR.

Based on the results presented in Tables 4 and 5, the high values of the PSNR obtained by the proposed method confirm that the MCs have indeed been enhanced and discriminated from the surrounding tissues (background).

Comparing with the PSNR of the original ROI and CLAHE ROI, we notice that CLAHE did not improve the contrast of MCs in the surrounding tissue. On the other hand, the proposed method has given very effective results even in comparison with literature where the difference is great.

3.3 MCs detection rate

The performance of the proposed method was also evaluated by the sensitivity parameter.

$$sens = \frac{TP}{TP + FN} \tag{6}$$

The *TP* are the number of MCs detected by the proposed method and *FN* are the number of MCs not detected according to the expert's annotations. For this, a segmentation of enhanced ROIs was done. According to the histogram of enhanced ROI, MCs are characterised by an intensity greater than '200', so the threshold is fixed at this value to obtain a binary ROI, followed by a dilatation with a structuring element of disc shape and size 1 (Figure 18).

Figure 18 Segmentation of MCs, (a) enhanced ROI (b) histogram of ROI (c) segmentation of MC based on thresholding (see online version for colours)

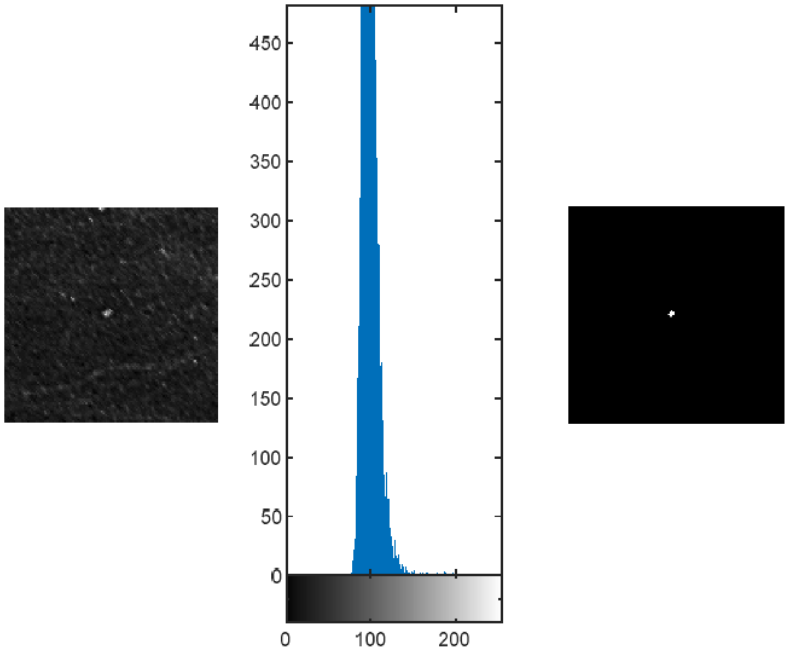

(a) (b) (c)

The results of Table 6 show that for class A where the breast density is low, the sensitivity of detection reached a rate of 95.33%. We note that this sensitivity decreased with the increase of breast density to 92.59% but remains a high and efficient rate, particularly for classes C and D where MCs are difficult to locate because of the low contrast between them and the surrounding tissue.

Table 6 MCs sensitivity of each BI-RADS class

BI-RADS class	*A < 25%*	*25 < B < 50%*	*50 < C < 75%*	*D > 75%*
Basile et al. (2019)	88.89%	95%	90.66%	92.50%
Proposed method	**95.33%**	**94.88%**	**93.60%**	**92.59%**

By comparing with results obtained in Basile et al. (2019) where the authors used the Hough transform for the detection of MCs clusters of the BCDR database, our method shows its performance especially for classes A and C where the difference is remarkable. Overall, the results in Table 7 show that the proposed method was able to detect MCs with a sensitivity of 94.20% for the INbreast database, 91.30% for the mini-MIAS database and 92.5% for the DDSM database, note that the 40 mammograms of the latter are of breast density greater than 50% (classes C and D).

Figure 19 MCs detection results, (a) original ROIs (b) ROIs with expert annotations (c) MCs detection with proposed method (d) segmented MCs

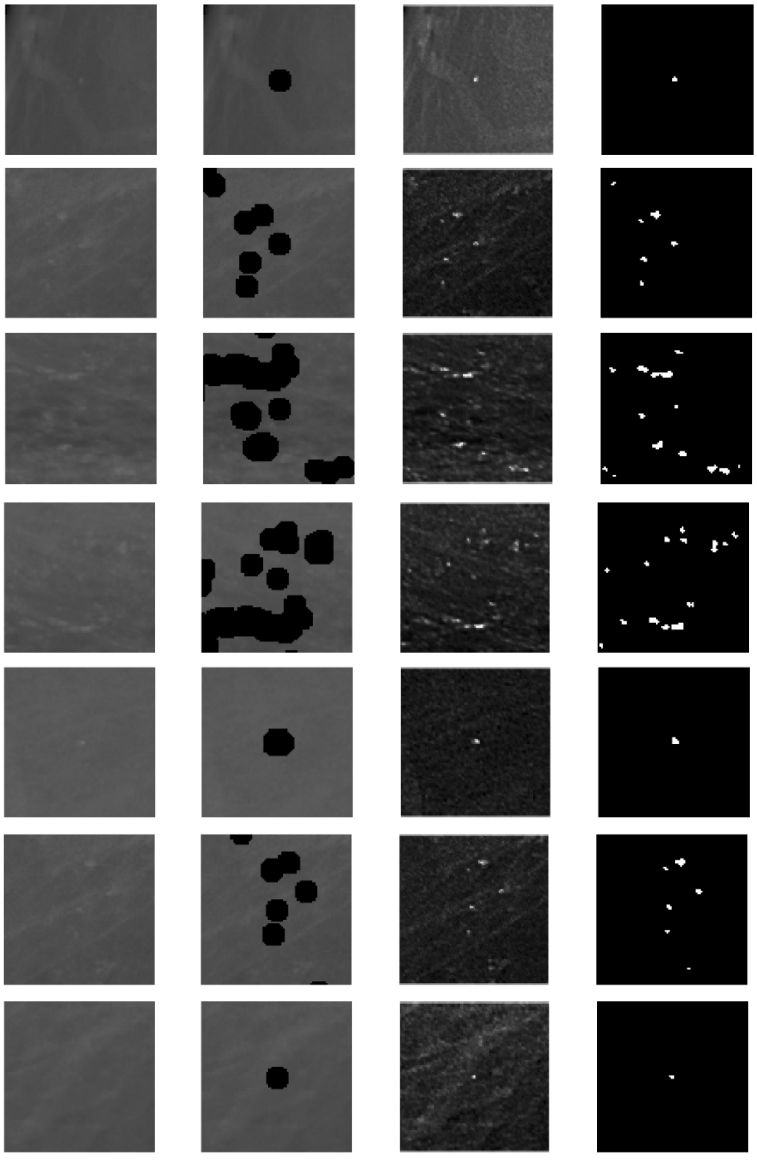

In order to compare the performance of our method with the literature, we considered recent works using different databases and a different number of data. The proposed method shows its performance in terms of sensitivity with a minimum of 91.30% and a maximum of 94.20% compared to the state of art reported in Table 7. The sensitivity reported in Basile et al. (2019) of 91.78% is limited given the large number of images used for detection of only clusters of MCs knowing that the clusters are easier to detect compared to MCs individually distributed. In Rubio et al. (2019), the proposed algorithm

has reached a good rate of 94.71% for the mini-MIAS database but a rate of 88.81% for the DDSM database with 100 images which is a reduced rate compared to our method. Finally, in Savelli et al. (2020), the INbreast database was used for the detection of MCs using a multi-context CNN. A sensitivity of 83.54% has been reported which is a low rate of over 10% compared to our method, note that these models are based on deep learning and require a large number of labelled data and powerful hardware to minimise the computation time.

Table 7 Compared sensitivity values with literature

Research	*Database*	*Number of data*	*Sensitivity*
Basile et al. (2019)	BCDR	364	91.78%
Rubio et al. (2019)	Mini-MIAS	23	94.71%
	DDSM	100	88.81%
Savelli et al. (2020)	INbreast	301	83.54%
Proposed method	Mini-MIAS	**23**	**91.30%**
	DDSM	**40**	**92.5%**
	INbreast	**308**	**94.20%**

4 Conclusions

The MCs are the first signs of precancerous cells. Given their small size, radiologists have difficulties to identify them, particularly when it concerns dense breasts.

This paper presents a method for the MCs detection. The originality of this approach consists in two steps: the pre-processing step where we were inspired by haze removal algorithm used in atmospheric images by considering breast density as haze that masks MCs. The second processing step is based on multifractal measures which have highlights the MCs in relation to the surrounding tissue which is the background.

The proposed method shows its performance in comparison with the different methods proposed in the literature. The considerable results of the PSNR prove that the contrast of the MCs has indeed been improved and the MCs are well discriminated from the background, which facilitates their detection and localisation. These results are striking in the case of dense tissues where very high values have been observed. The performance of our method also remained remarkable in terms of sensitivity.

This work must be continued for the characterisation and classification of MCs. On the other hand, the proposed method can be generalised as a method of mammograms processing for the detection of different breast lesions such as masses and architectural distortions.

References

Abdallah, Y.M.Y., Elgak, S., Zain, H. et al. (2018) 'Breast cancer detection using image enhancement and segmentation algorithms', *Biomedical Research*, Vol. 29, No. 20, pp.3732–3736.

Alam, N., Oliver, A., Denton, E.R.E. et al. (2018) 'Automatic segmentation of microcalcification clusters', in *Annual Conference on Medical Image Understanding and Analysis*, Springer, Cham, pp.251–261.

Al-Antari, M.A., Al-Masni, M.A. and Kim, T-S. (2020) 'Deep learning computer-aided diagnosis for breast lesion in digital mammogram', in *Deep Learning in Medical Image Analysis*, pp.59–72, Springer, Cham.

Alasadi, A.H.H. and Al-Saedi, A.K.H. (2017) 'A method for microcalcifications detection in breast mammograms', *Journal of Medical Systems*, Vol. 41, No 4, p.68.

Atupelage, C., Nagahashi, H., Yamaguchi, M. et al. (2013) 'Computational grading of hepatocellular carcinoma using multifractal feature description', *Computerized Medical Imaging and Graphics*, Vol. 37, No. 1, pp.61–71.

Azam, A.S.B., Malek, A.A., Ramlee, A.S. et al. (2020) 'Segmentation of breast microcalcification using hybrid method of canny algorithm with otsu thresholding and 2D wavelet transform', in *2020 10th IEEE International Conference on Control System, Computing and Engineering (ICCSCE)*, IEEE, pp.91–96.

Bagchi, S., Tay, K.G., Huong, A. et al. (2020) 'Image processing and machine learning techniques used in computer-aided detection system for mammogram screening – a review', *International Journal of Electrical and Computer Engineering*, Vol. 10, No 3, p.2336.

Baravalle, R., Thomsen, F., Delrieux, C. et al. (2017) 'Three-dimensional multifractal analysis of trabecular bone under clinical computed tomography', *Medical Physics*, Vol. 44, No. 12, pp.6404–6412.

Basile, T.M.A., Fanizzi, A., Losurdo, L. et al. (2019) 'Microcalcification detection in fullfield digital mammograms: a fully automated computer-aided system', *Physica Medica*, Vol. 64, pp.1–9.

Bhat, M., Patil, M.S.T., Shrinivas, M.P. et al. (2017) 'Automated retinal optic disc detection using pixel based multi fractal analysis', in *2017 International Conference on Computer, Communication and Signal Processing (ICCCSP)*, IEEE, pp.1–8.

Bhateja, V., Misra, M. and Urooj, S. (2020) *Non-Linear Filters for Mammogram Enhancement*, Springer, Singapore.

Chen, D-R., Chang, R-F., Chen, C-J. et al. (2005) 'Classification of breast ultrasound images using fractal feature', *Clinical Imaging*, Vol. 29, No. 4, pp.235–245.

Chianghau, T.A.Y. (2012) *Algorithms for Tissue Image Analysis using Multifractal Techniques*, Doctoral dissertation, University of Canterbury.

Ciecholewski, M. (2017) 'Microcalcification segmentation from mammograms: a morphological approach', *Journal of Digital Imaging*, Vol. 30, No. 2, pp.172–184.

Datta, D. and Sathish, S. (2019) 'Application of fractals to detect breast cancer', in *Journal of Physics: Conference Series*, IOP Publishing, p.012030.

Ding, Y., Pardon, M.C., Agostini, A. et al. (2016) 'Novel methods for microglia segmentation, feature extraction, and classification', *IEEE/ACM Transactions on Computational Biology and Bioinformatics*, Vol. 14, No. 6, pp.1366–1377.

Eltrass, A.S. and Salama, M.S. (2019) 'Fully automated scheme for computer-aided detection and breast cancer diagnosis using digitised mammograms', *IET Image Processing*, Vol. 14, No 3, pp.495–505.

Gerasimova-Chechkina, E., Toner, B., Marin, Z. et al. (2016) 'Comparative multifractal analysis of dynamic infrared thermograms and X-ray mammograms enlightens changes in the environment of malignant tumors', *Frontiers in Physiology*, Vol. 7, p.336.

Hadjidj, I., Feroui, A., Belgherbi, A. et al. (2019) 'Microcalcifications segmentation from mammograms for breast cancer detection', *International Journal of Biomedical Engineering and Technology*, Vol. 29, No. 1, pp.1–16.

Hamed, G., Marey, M.A.E-R., Amin, S.E-S. et al. (2020) 'Deep learning in breast cancer detection and classification', in *Joint European-US Workshop on Applications of Invariance in Computer Vision*, pp.322–333, Springer, Cham.

He, K., Sun, J. and Tang, X. (2010) 'Single image haze removal using dark channel prior', *IEEE Transactions on Pattern Analysis and Machine Intelligence*, Vol. 33, No. 12, pp.2341–2353.

Heath, M., Bowyer, K., Kopans, D. et al. (1998) 'Current status of the Digital Database For Screening Mammography', in *Digital Mammography*, pp.457–460, Springer, Dordrecht.

Jayasuriya, S.A., Liew, A.W-C. and Law, N-F. (2013) 'Brain symmetry plane detection based on fractal analysis', *Computerized Medical Imaging and* Graphics, Vol. 37, Nos. 7–8, pp.568–580.

Kestener, P. (2003) *Analyse multifractale 2D et 3D à l'aide de la transformation en ondelettes: application en mammographie et en turbulence développée*, Thèse de doctorat. Université Sciences et Technologies-Bordeaux I.

Kestener, P., Lina, J.M., Saint-Jean, P. et al. (2001) 'Wavelet-based multifractal formalism to assist in diagnosis in digitized mammograms', *Image Analysis & Stereology*, Vol. 20, No. 3, pp.169–174.

Khider, M. (2011) *Analyse multifractale par MMTO-2D évaluation sur des images radar et médicales*, Thèse de doctorat.

Li, H., Giger, M.L., Olopade, O.I. et al. (2007) 'Fractal analysis of mammographic parenchymal patterns in breast cancer risk assessment', *Academic Radiology*, Vol. 14, No. 5, pp.513–521.

LolaCosta, E.V. and Nogueira, R.A. (2015) 'Fractal, multifractal and lacunarity analysis applied in retinal regions of diabetic patients with and without nonproliferative diabetic retinopathy', *Fractal Geom. Nonlinear Anal. Med. Biol.*, Vol. 1, No. 3, pp.112–119.

Lopez, M.A.G., Posada, N., Moura, D.C. et al. (2012) 'BCDR: a Breast Cancer Digital Repository', in *15th International Conference on Experimental Mechanics*.

Mandelbrot, B.B. (1975) *Les objets fractals: forme, hasard et dimension*, Flammarion, Paris.

Marin, Z., Batchelder, K.A., Toner, B.C. et al. (2017) 'Mammographic evidence of microenvironment changes in tumorous breasts', *Medical Physics*, Vol. 44, No. 4, pp.1324–1336.

Mohammed, M.A., Al-Khateeb, B., Rashid, A.N. et al. (2018) 'Neural network and multi-fractal dimension features for breast cancer classification from ultrasound images', *Computers & Electrical Engineering*, Vol. 70, pp.871–882.

Moreira, I.C., Amaral, I., Domingues, I. et al. (2012) 'Inbreast: toward a full-field digital mammographic database', *Academic Radiology*, Vol. 19, No. 2, pp.236–248.

Mutlu, F., Çetinel, G. and Gül, S. (2020) 'A fully-automated computer-aided breast lesion detection and classification system', *Biomedical Signal Processing and Control*, Vol. 62, p.102157.

Quintanilla-Domínguez, J., Ruiz-Pinales, J., Barrón-Adame, J.M. et al. (2018) 'Microcalcifications detection using image processing', *Computación y Sistemas*, Vol. 22, No. 1, pp.291–300.

Rajković, N., Kolarević, D., Kanjer, K. et al. (2016) 'Comparison of monofractal, multifractal and gray level co-occurrence matrix algorithms in analysis of breast tumor microscopic images for prognosis of distant metastasis risk', *Biomedical Microdevices*, Vol. 18, No. 5, p.83.

Rajkovic, N., Radulovic, M., Stojadinovic, B. et al. (2017) 'Analysis of histopathology images by the use of monofractal and multifractal algorithms', in *2017 21st International Conference on Control Systems and Computer Science (CSCS)*, IEEE, pp.350–355.

Rangayyan, R.M. and Nguyen, T.M. (2005) 'Pattern classification of breast masses via fractal analysis of their contours', in *International Congress Series*, Elsevier, pp.1041–1046.

Rubio, Y., Montiel, O. and Sepúlveda, R. (2019) 'Quantum inspired algorithm for microcalcification detection in mammograms', *Information Sciences*, Vol. 480, pp.305–323.

Sahli, I.S., Bettaieb, H.A., Abdallah, A.B. et al. (2015) 'Detection and segmentation of microcalcifications in digital mammograms using multifractal analysis', in *2015 International Conference on Image Processing Theory, Tools and Applications (IPTA)*, IEEE, pp.180–184.

Sanchez-Montero, R., Martinez-Rojas, J-A., Lopez-Espi, P-L. et al. (2019) 'Filtering of mammograms based on convolution with directional fractal masks to enhance microcalcifications', *Applied Sciences*, Vol. 9, No. 6, p.1194.

Savelli, B., Bria, A., Molinara, M. et al. (2020) 'A multi-context CNN ensemble for small lesion detection', *Artificial Intelligence in Medicine*, Vol. 103, p.101749.

Singh, B. and Kaur, M. (2018) 'An approach for classification of malignant and benign microcalcification clusters', *Sadhana*, Vol. 43, No. 3, p.39.

Slim, I., Bettaieb, H., Abdallah, A.B. et al. (2019) 'Mulitifractal analysis with lacunarity for microcalcification segmentation', in *Digital Health Approach for Predictive, Preventive, Personalised and Participatory Medicine*, Springer, Cham, pp.33–41.

Stojić, T., Reljin, I. and Reljin, B. (2006) 'Adaptation of multifractal analysis to segmentation of microcalcifications in digital mammograms', *Physica A: Statistical Mechanics and its Applications*, Vol. 367, pp.494–508.

Ţălu, Ş., Călugăru, D.M. and Lupaşcu, C.A. (2015) 'Characterisation of human non-proliferative diabetic retinopathy using the fractal analysis', *International Journal of Ophthalmology*, Vol. 8, No. 4, p.770.

Ţălu, Ş., Stach, S., Călugăru, D.M. et al. (2017) 'Analysis of normal human retinal vascular network architecture using multifractal geometry', *International Journal of Ophthalmology*, Vol. 10, No. 3, p.434.

Tălu, S., Vlăduţiu, C. and Lupaşcu, C.A. (2015) 'Characterization of human retinal vessel arborisation in normal and amblyopic eyes using multifractal analysis', *International Journal of Ophthalmology*, Vol. 8, No 5, p.996.

Valvano, G., Santini, G., Martini, N. et al. (2019) 'Convolutional neural networks for the segmentation of microcalcification in mammography imaging', *Journal of Healthcare Engineering*, Vol. 2019, pp.1–9.

Vasiljevic, J., Pribic, J., Kanjer, K. et al. (2015) 'Multifractal analysis of tumour microscopic images in the prediction of breast cancer chemotherapy response', *Biomedical Microdevices*, Vol. 17, No. 5, p.93.

Verma, G., Luciani, M.L., Palombo, A. et al. (2018) 'Microcalcification morphological descriptors and parenchyma fractal dimension hierarchically interact in breast cancer: a diagnostic perspective', *Computers in Biology and Medicine*, Vol. 93, pp.1–6.

Wang, J. and Yang, Y. (2018) 'A context-sensitive deep learning approach for microcalcification detection in mammograms', *Pattern Recognition*, Vol. 78, pp.12–22.

Ward, W.O.C. and Bai, L. (2013) 'Multifractal analysis of microvasculature in health and disease', in *2013 35th Annual International Conference of the IEEE Engineering in Medicine and Biology Society (EMBC)*, IEEE, pp.2336–2339.

Yu, Y-e., Wang, F and Liu, L-l. (2015) 'Magnetic resonance image segmentation using multifractal techniques', *Applied Surface Science*, Vol. 356, pp.266–272.

Zyout, I. and Togneri, R. (2018) 'A computer-aided detection of the architectural distortion in digital mammograms using the fractal dimension measurements of BEMD', *Computerized Medical Imaging and Graphics*, Vol. 70, pp.173–184.